


Cite this: *RSC Adv.*, 2023, 13, 27984

# NiFe<sub>2</sub>O<sub>4</sub>@SiO<sub>2</sub>–Cu as a novel and efficient magnetically recoverable nanocatalyst for regioselective synthesis of β-thiol-1,2,3-triazoles under benign conditions†

Ronak Eisavi \* and Seiran Ghadernejad

A green, mild and eco-friendly approach for the three component one-pot regioselective synthesis of 1,2,3-triazoles from thiiranes has been introduced in the presence of NiFe<sub>2</sub>O<sub>4</sub>@SiO<sub>2</sub>–Cu as a new and recoverable nanocatalyst. First, the NiFe<sub>2</sub>O<sub>4</sub> nanoparticles have been produced through a solid-state reaction of hydrated nickel sulfate, hydrated iron(III) nitrate, NaOH and NaCl salts, and then calcined at 700 °C. Next, in order to protect the ferrite particles from oxidation and aggregation, the NiFe<sub>2</sub>O<sub>4</sub> was core-shelled using tetraethyl orthosilicate (TEOS) and converted to NiFe<sub>2</sub>O<sub>4</sub>@SiO<sub>2</sub>. Finally, the novel NiFe<sub>2</sub>O<sub>4</sub>@SiO<sub>2</sub>–Cu nanocomposite was successfully prepared by adding copper(II) chloride solution and solid potassium borohydride. The catalyst has been characterized by FT-IR, SEM, EDX, VSM, ICP-OES, TEM and XRD techniques. The 1,3-dipolar cyclization of 1,2,3-triazoles was performed successfully in water at room temperature in high yields. The recoverability and reusability of the heterogeneous NiFe<sub>2</sub>O<sub>4</sub>@SiO<sub>2</sub>–Cu have also been investigated using VSM, SEM and FT-IR analyses. The catalyst was used four times in consecutive runs without considerable loss of activity. The presented procedure provides significant benefits such as using water as a green solvent, absence of hazardous organic solvents, high yields, benign conditions and recyclability of the magnetic catalyst.

Received 10th August 2023  
Accepted 13th September 2023

DOI: 10.1039/d3ra05433k

rsc.li/rsc-advances

## 1. Introduction

Multi-component reactions (MCRs), in which three or more reactants react to produce only one product, provide an easy and practical process for generating intricate molecules with structural complexity.<sup>1</sup> The eco-friendliness, perfect regioselectivity high product yields, short reaction time and convenience of the method are among the benefits of these types of reactions.

Moreover, one-pot reactions have recently received a lot of attention in various fields such as industrial chemistry, organic synthesis, biomedical, production of bioactive reagents, pharmaceutical investigations and drug discovery.<sup>2–5</sup> These reactions provide excellent facilities for versatile preparation of a wide diversity of organic compounds especially biologic active molecules which have benefits such as high atom economy, escape of time-consuming protection-deprotection steps, making them certainly better than classical multi-step synthetic

procedures.<sup>6–9</sup> These approaches are effective because several synthetic transformations and bond-forming steps can be carried out in a single pot, while circumventing several purification procedures at the same time. A one-pot procedure can thus minimize chemical waste, save time, and simplify practical aspects.<sup>10–12</sup> Furthermore, in the growing field of organocatalysis,<sup>13</sup> organocatalysts are extremely effective reagents in achieving a one-pot, multi-step synthesis. This is evidenced by a dramatic increase of impressive syntheses over the past decade.<sup>14–17</sup>

1,2,3-Triazoles have been considered as one of the most prominent and substantial intermediates in pharmaceutical and biological industries. They show unique activities such as antioxidants, analgesic, antimicrobial, anti HIV, anticancer, local anaesthetic, anticonvulsant, antiproliferative, antiallergic, antiviral, antitubercular, antifungal, antibacterial, anti-inflammatory and antimalarial.<sup>18–26</sup>

Recently, the Huisgen 1,3-dipolar cycloaddition between azides and alkynes has been utilized to manufacture the 1,2,3-triazoles.<sup>27</sup> Although, one-pot synthesis of β-hydroxy-1,2,3-triazoles has been reported using click reaction of azides, alkynes and epoxides catalyzed by copper catalysts,<sup>28–43</sup> but the use of thiiranes in the mentioned reaction has been investigated only in two cases.<sup>44,45</sup>

Department of Chemistry, Payame Noor University, P.O. BOX 19395-4697, Tehran, Iran. E-mail: r\_eisavi@pnu.ac.ir

† Electronic supplementary information (ESI) available: FT-IR, <sup>1</sup>H NMR and <sup>13</sup>C NMR spectral information of β-thiol-1,4-disubstituted-1,2,3-triazoles. See DOI: <https://doi.org/10.1039/d3ra05433k>



Recently, the diverse synthetic reactions have been improved and facilitated using heterogeneous catalysts.<sup>46–48</sup> Moreover, magnetic nanoparticles have received great attention as green heterogeneous catalysts in organic synthesis due to their convenient synthesis, easy separation, high degree of catalytic activity and chemical stability, operational simplicity, eco-friendliness, and recoverability using an external magnetic field without the need for filtration and leaching or loss of the catalyst.<sup>49–51</sup>

However, the nano-ferrites always suffer from adsorption problems because they have a large surface to volume ratio and can develop strong magnetic attractions that lead to self-aggregation and a decrease in the amount of functional groups on the surface.<sup>52</sup>

To prevent agglomeration of magnetic nanoparticles and improve their efficiency, their surfaces could be modified using various materials such as silica, metals, polymers, metal oxides, surfactant, *etc.*<sup>53</sup> The coating of nano-ferrites with a functionalized shell, not only reduces the aggregation of the nanoparticles in the solution, but also improves the efficiency of the catalyst by increasing the amount of functional groups on the surface. Furthermore, in recent years, the nanostructures coated with silica, metal and metal oxides have been widely used as selective detector of biochemical substances,<sup>54,55</sup> easy separable catalysts in organic transformations, and smart nanomaterials utilized in the biomedical area to develop the role of biosynthesized nanoparticles for ameliorating human health through broad applications in the targeted drug delivery, controlled release drug delivery, wound dressing, tissue scaffolding, and medical implants.<sup>56–58</sup>

In continuation of our research on the successful synthesis of magnetic nanoparticles,<sup>59–64</sup> herein, we would like to introduce the novel recoverable  $\text{NiFe}_2\text{O}_4@\text{SiO}_2\text{-Cu}$  nanocatalyst for the three-component regioselective procedure for synthesis of  $\beta$ -thiol-1,4-disubstituted-1,2,3 triazoles from sodium azide, thiiranes, and terminal alkynes in water at room temperature (Scheme 1).

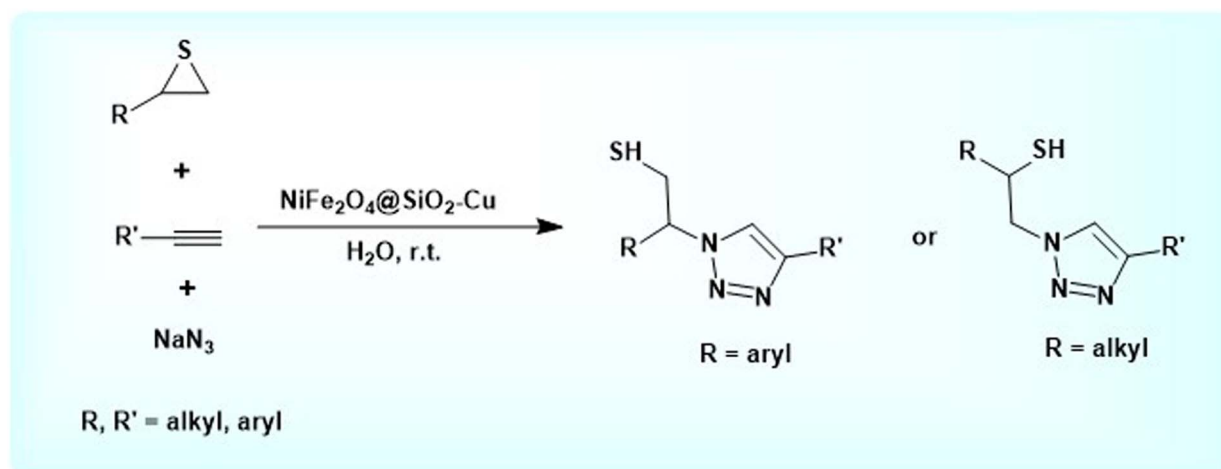
## 2. Experimental

### 2.1. Materials and instruments

All chemical substrates were purchased from the Merck and Aldrich Chemical Companies and were used without further purification. FT-IR spectra were obtained by Thermo Nicolet Nexus 670 FT-IR, and  $^1\text{H}/^{13}\text{C}$  NMR spectra were recorded on 500 MHz Bruker Avance spectrometer. HRMS analyses were also performed in the electron impact mode (EI) at 70 eV. Magnetic properties of nanoparticles were measured by a VSM (Meghnatis Daghigh Kavir Co., Kashan Kavir, Iran) at room temperature. Melting points were measured on an Electrothermal IA9100 microscopic digital melting point apparatus. Morphology and size distribution of the particles were examined by TEM using an EM10C-100 kV series microscope from the Zeiss Company, Germany. FESEM images were obtained using FESEM-TESCAN. The energy dispersive X-ray spectrometer (EDS) analysis was taken on a MIRA3 FE-SEM microscope (TESCAN, Czech Republic) equipped with an EDS detector (Oxford Instruments, UK). The crystalline structure of the catalyst was studied by X-ray diffraction on a Bruker D8-Advanced diffractometer with graphite-monochromatized  $\text{Cu K}\alpha$  radiation ( $\lambda = 1.54056 \text{ \AA}$ ) at room temperature. The Cu content on the catalyst was determined by PerkinElmer Optima 7300DV ICP-OES analyzer.

### 2.2. Synthesis of $\text{NiFe}_2\text{O}_4$

$\text{NiFe}_2\text{O}_4$  nanoparticles were synthesized by a solid-state method according to our previously reported procedures.<sup>59</sup> Concisely, in an agate mortar,  $\text{NiSO}_4 \cdot 6\text{H}_2\text{O}$  (0.31 g, 2 mmol),  $\text{Fe}(\text{NO}_3)_3 \cdot 9\text{H}_2\text{O}$  (1.61 g, 4 mmol),  $\text{NaOH}$  (0.64 g, 16 mmol), and  $\text{NaCl}$  (0.232 g, 4 mmol) were placed in a molar ratio of 1 : 2 : 8 : 2 and ground for 1 hour. After 5 minutes of grinding, the mixture turned into a brown paste. The reaction proceeded with the release of heat. The reaction was completed in one hour. In order to remove the extra salts, the doughy mixture was washed with distilled water several times, and then it was dried at 80 °C for 2 h. The



Scheme 1 Synthesis of  $\beta$ -thiol-1,2,3-triazoles from thiiranes catalyzed by  $\text{NiFe}_2\text{O}_4@\text{SiO}_2\text{-Cu}$ .

obtained product was calcined at 700 °C for 2 hours to afford the pure  $\text{NiFe}_2\text{O}_4$  nanoparticles as a brown powder.

### 2.3. Preparation of $\text{NiFe}_2\text{O}_4@\text{SiO}_2$

The surface of nickel ferrite nanoparticles was silica coated through an amended sol-gel procedure.<sup>64</sup> First,  $\text{NiFe}_2\text{O}_4$  (0.5 g) was added to a solution of ethanol (50 mL), distilled water (10 mL) and ammonium hydroxide (2.5 mL, 25%) and ultrasonicated for 2 h. Then 1.5 mL of tetraethyl orthosilicate (TEOS) was added dropwise to the prepared mixture and sonicated for a further 20 min. After continuous stirring at room temperature for 24 h, the  $\text{NiFe}_2\text{O}_4@\text{SiO}_2$  particles were collected, washed several times with distilled water and dried in an oven at 100 °C for 20 h.

### 2.4. Preparation of $\text{NiFe}_2\text{O}_4@\text{SiO}_2\text{-Cu}$ nanocomposite

First,  $\text{NiFe}_2\text{O}_4@\text{SiO}_2$  (1 g) was added to a solution of  $\text{CuCl}_2 \cdot 2\text{H}_2\text{O}$  (0.68 g, 4 mmol) in distilled water (50 mL). The mixture was stirred strongly for 30 min and then  $\text{KBH}_4$  powder (0.1 g) was added gradually to reduce  $\text{Cu}^{2+}$  cations and produce the Cu nanoparticles. After continues stirring of the mixture for 1 hour at room temperature, the  $\text{NiFe}_2\text{O}_4@\text{SiO}_2\text{-Cu}$  nanocomposite was generated and separated using a magnet, washed with distilled water and finally dried under air atmosphere.

### 2.5. Synthesis of thiiranes from epoxides: a general procedure

The different thiiranes were prepared using a previously reported solvent-free method.<sup>65</sup> Briefly, a mixture of epoxide (1 mmol) and alumina supported thiourea (0.752 g, 25% w/w) was placed in a mortar and ground at room temperature. The progress of the reaction was tracked by TLC using *n*-hexane : EtOAc (10 : 4) as an eluent. After completion of the reaction, the mixture was washed with ethylacetate. Next, the washing solvents were evaporated under reduced pressure to obtain the crude thiirane, which was then purified using a short-column chromatography over silica gel.

### 2.6. Synthesis of $\beta$ -thiol-1,2,3-triazoles from thiiranes catalyzed by $\text{NiFe}_2\text{O}_4@\text{SiO}_2\text{-Cu}$ in water at room temperature: a general procedure

A solution of the thiirane (1 mmol), alkyne (1 mmol) and  $\text{NaN}_3$  (0.078 g, 1.2 mmol) in  $\text{H}_2\text{O}$  (5 mL) was placed in a round-bottomed flask equipped with a magnetic stirrer. After adding the  $\text{NiFe}_2\text{O}_4@\text{SiO}_2\text{-Cu}$  nanocatalyst (0.02 g) to the solution, the

mixture was stirred for an appropriate time at room temperature. The completion of the reaction was evaluated by TLC using *n*-hexane : EtOAc (10 : 2) as an eluent. Then, the nanocatalyst was separated applying an external magnetic field and accumulated for the next cycle. To obtain the product, the reaction mixture was extracted with ethyl acetate and then dried over anhydrous  $\text{Na}_2\text{SO}_4$ . The organic solvent was evaporated and the crude  $\beta$ -thiol-1,4-disubstituted-1,2,3-triazole was produced. The  $\beta$ -thiol-1,4-disubstituted-1,2,3-triazoles derivatives were purified through recrystallization with EtOH/ $\text{H}_2\text{O}$  (1 : 1), and then characterized by HRMS (EI), FT-IR,  $^1\text{H}$  NMR and  $^{13}\text{C}$  NMR spectra. All products are known compounds and were confirmed by comparison of their spectra with those of valid samples;<sup>44,45</sup> these data are given in the ESI.†

### 2.7. Recycling of $\text{NiFe}_2\text{O}_4@\text{SiO}_2\text{-Cu}$ nanocatalyst

After completion of the reaction, the magnetic nanoparticles of  $\text{NiFe}_2\text{O}_4@\text{SiO}_2\text{-Cu}$  were separated using a simple magnet, washed several times with ethyl acetate, and dried under air atmosphere. The collected nanoparticles were reused in the next run without any remarkable loss of magnetic property or catalytic activity.

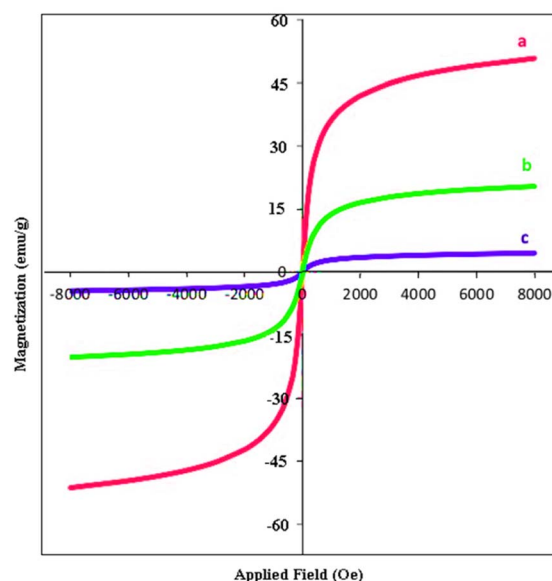
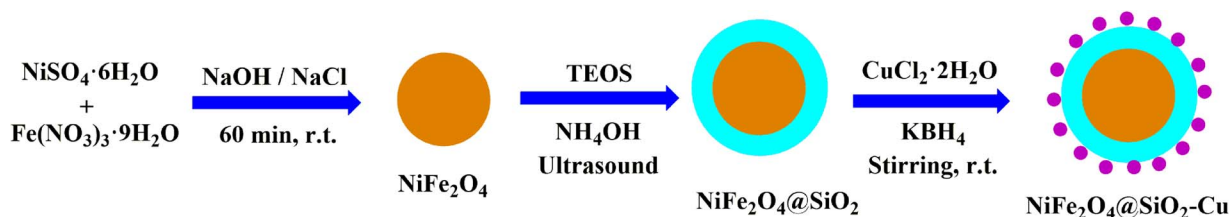


Fig. 1 Magnetization curves of (a)  $\text{NiFe}_2\text{O}_4$ , (b)  $\text{NiFe}_2\text{O}_4@\text{SiO}_2$  and (c)  $\text{NiFe}_2\text{O}_4@\text{SiO}_2\text{-Cu}$ .



Scheme 2 Synthesis of  $\text{NiFe}_2\text{O}_4@\text{SiO}_2\text{-Cu}$  nanocomposite.



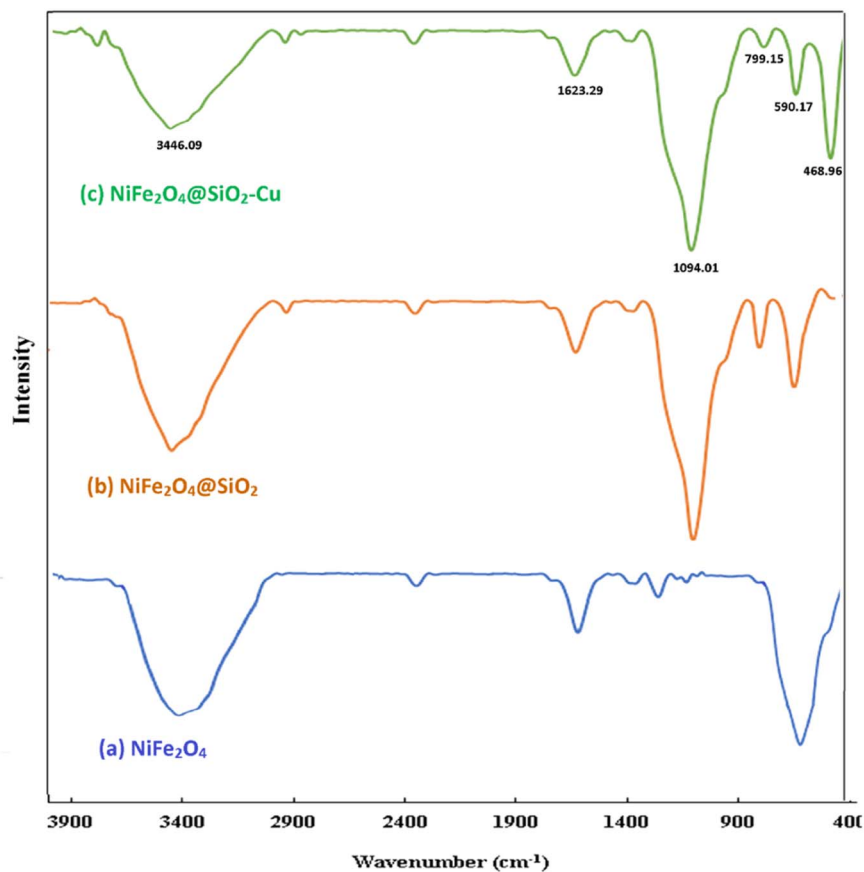


Fig. 2 FT-IR (KBr) spectra of (a)  $\text{NiFe}_2\text{O}_4$ , (b)  $\text{NiFe}_2\text{O}_4@\text{SiO}_2$  and (c)  $\text{NiFe}_2\text{O}_4@\text{SiO}_2\text{-Cu}$ .

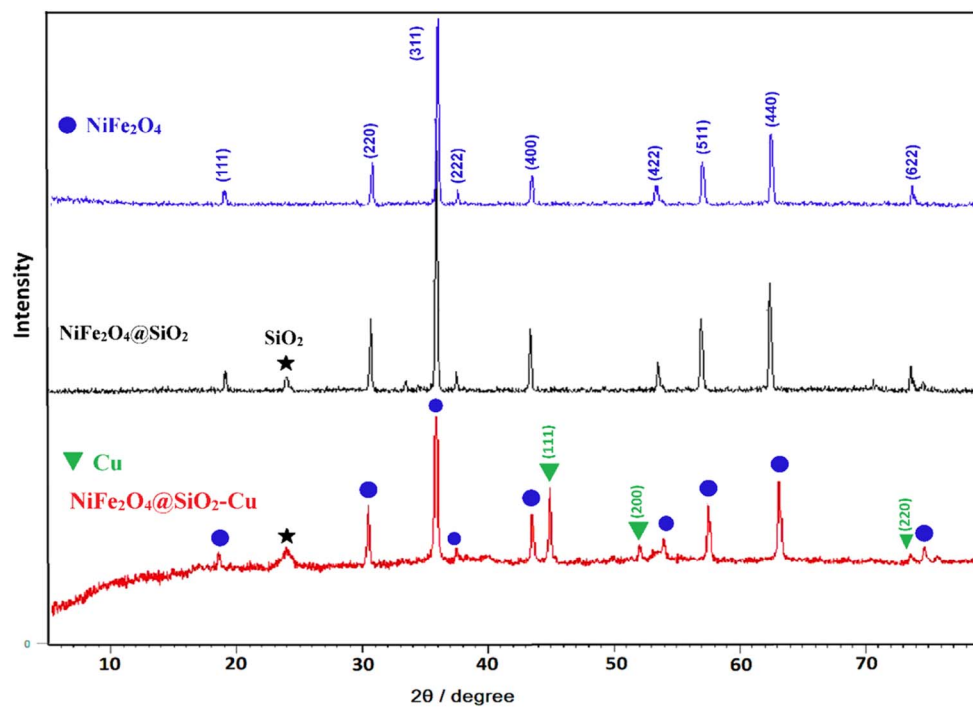


Fig. 3 XRD patterns of  $\text{NiFe}_2\text{O}_4$ ,  $\text{NiFe}_2\text{O}_4@\text{SiO}_2$  and  $\text{NiFe}_2\text{O}_4@\text{SiO}_2\text{-Cu}$ .



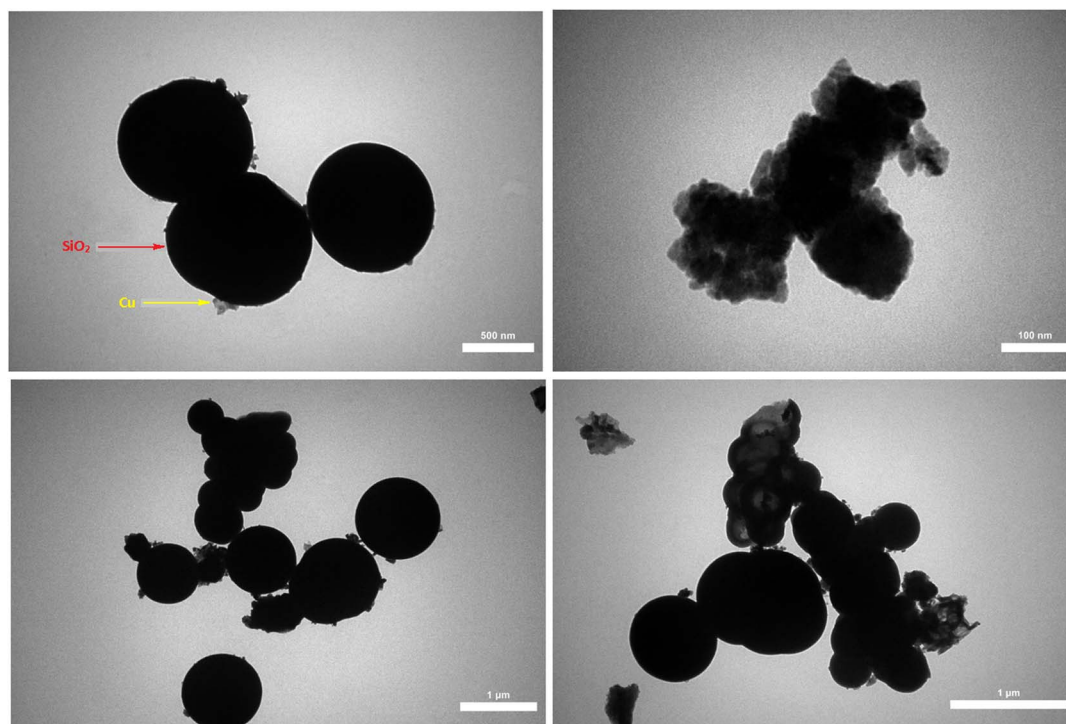


Fig. 4 TEM images of  $\text{NiFe}_2\text{O}_4@\text{SiO}_2\text{-Cu}$ .

### 3. Results and discussion

#### 3.1. Synthesis and characterization of $\text{NiFe}_2\text{O}_4@\text{SiO}_2\text{-Cu}$ nanocatalyst

Nickel ferrite nanoparticles with a large surface to volume ratio have high catalytic activity. However, they tend to aggregate and

agglomerate, which subsequently leads to minimize the surface energies. The naked ferrite nanoparticles due to their high chemical activity are easily oxidized in air, which usually resulting in loss of magnetic property and the reduction of their dispersity. Therefore, coating of their surface with an inorganic layer such as silica, metal or nonmetal elementary substances is

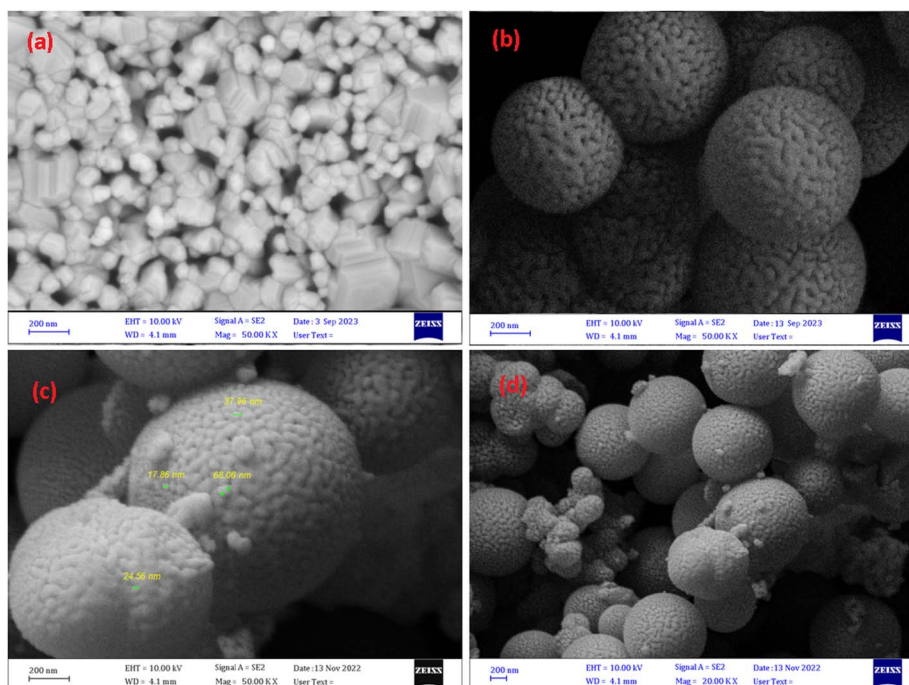


Fig. 5 FESEM images of (a)  $\text{NiFe}_2\text{O}_4$ , (b)  $\text{NiFe}_2\text{O}_4@\text{SiO}_2$ , (c) and (d)  $\text{NiFe}_2\text{O}_4@\text{SiO}_2\text{-Cu}$ .



useful. The protecting shells not only prevent the accumulation of the particles in the solution, but also improve the efficiency of the catalyst by providing the more functional groups on its surface.<sup>45,64</sup> Easy separation, recyclability, and reusability are among the advantages of nickel magnetic ferrites, which make them suitable supports for the synthesis of nanocomposites.

NiFe<sub>2</sub>O<sub>4</sub>@SiO<sub>2</sub>-Cu was prepared in a three-step process (Scheme 2). The new synthesized NiFe<sub>2</sub>O<sub>4</sub>@SiO<sub>2</sub>-Cu nanocatalyst was characterized by diverse methods such as vibration sample magnetometer (VSM), FT-IR, transmission electron microscopy (TEM), X-ray diffraction (XRD), field emission scanning electron microscope (FESEM), energy dispersive X-ray spectrometer (EDS), and inductively coupled plasma optical emission spectrometry (ICP-OES).

**3.1.1. Vibration sample magnetometer (VSM).** Magnetic properties of NiFe<sub>2</sub>O<sub>4</sub>, NiFe<sub>2</sub>O<sub>4</sub>@SiO<sub>2</sub> and NiFe<sub>2</sub>O<sub>4</sub>@SiO<sub>2</sub>-Cu nanoparticles were investigated by the vibrating sample magnetometer (VSM). The narrow cycles with low coercivity indicate the typical ferromagnetic behavior of the soft magnetic materials at room temperature. The saturation magnetization

( $M_s$ ) value of NiFe<sub>2</sub>O<sub>4</sub>, NiFe<sub>2</sub>O<sub>4</sub>@SiO<sub>2</sub> and NiFe<sub>2</sub>O<sub>4</sub>@SiO<sub>2</sub>-Cu was around 50, 21 and 5 emu g<sup>-1</sup>, respectively. Hence, the amount of  $M_s$  and the magnetic property are reduced by coating one layer on another. This is due to the presence of nonmagnetic layers of silica and copper in the nanocomposite structure (Fig. 1).

**3.1.2. Fourier transform infra-red (FT-IR) spectrum.** The functional groups in the magnetic nanoparticles of NiFe<sub>2</sub>O<sub>4</sub>, NiFe<sub>2</sub>O<sub>4</sub>@SiO<sub>2</sub> and NiFe<sub>2</sub>O<sub>4</sub>@SiO<sub>2</sub>-Cu were identified by the FT-IR spectroscopy (Fig. 2). The absorption peak at 590 cm<sup>-1</sup> belongs to the vibration of metal oxide bonds (Fe-O and Ni-O) which shows the presence of NiFe<sub>2</sub>O<sub>4</sub> nanoparticles. The absorption bands at 3446 and 1623 cm<sup>-1</sup> correspond to the O-H stretching and bending modes in the adsorbed water, respectively.<sup>62</sup>

The broad bands at 1094 and 799 cm<sup>-1</sup> are related to the asymmetrical and symmetrical stretching vibrations of Si-O-Si, which confirm the presence of silica layers in the composite. An absorption peak appeared at 468 cm<sup>-1</sup> is attributed to the bending vibrations of O-Si-O.<sup>66</sup> The band corresponding to Cu-

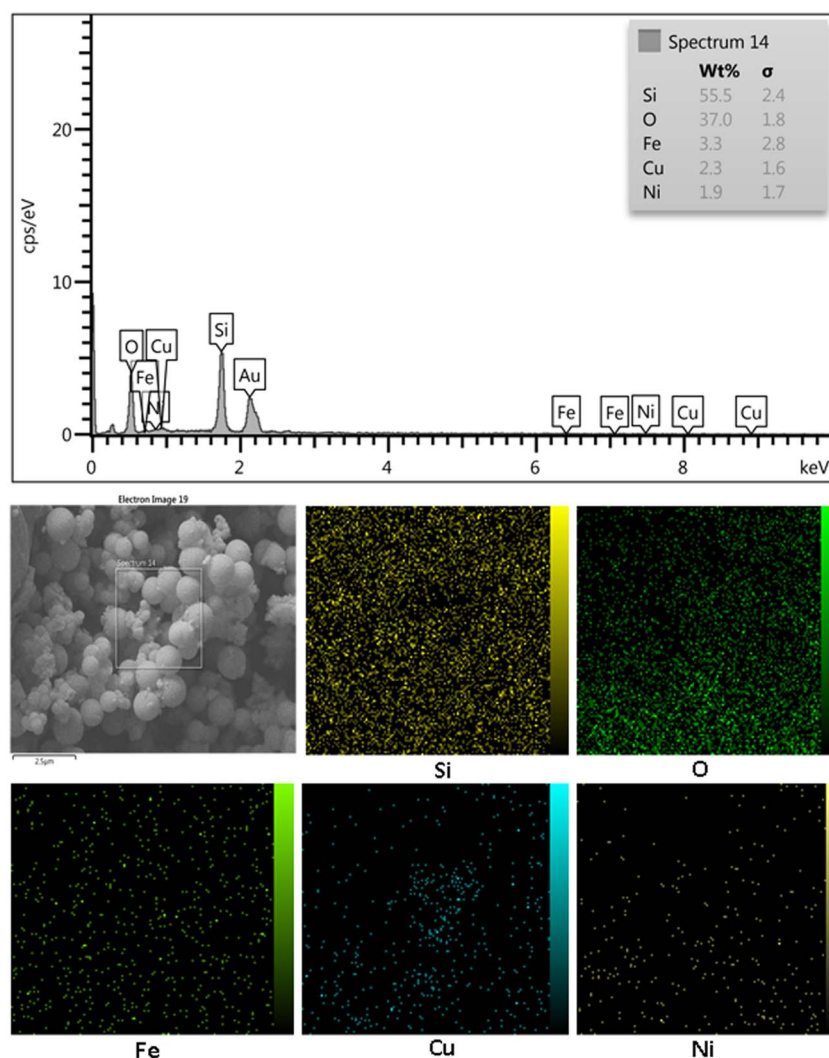


Fig. 6 EDS of NiFe<sub>2</sub>O<sub>4</sub>@SiO<sub>2</sub>-Cu and elemental mapping of Fe, Ni, O, Si, Cu.

**Table 1** Three-component reaction of styrene episulfide with phenylacetylene and sodium azide catalysed by  $\text{NiFe}_2\text{O}_4@\text{SiO}_2\text{-Cu}$  under different conditions<sup>a</sup>

Entry	$\text{NiFe}_2\text{O}_4@\text{SiO}_2\text{-Cu}$ (g)	Solvent	Time (h)	Yield <sup>b</sup> (%)
1	—	$\text{H}_2\text{O}$	20	0
2	0.01	$\text{H}_2\text{O}$	10	50
3	0.015	$\text{H}_2\text{O}$	10	80
4	0.02	$\text{H}_2\text{O}$	8	98
5	0.03	$\text{H}_2\text{O}$	8	98
6	0.02	$\text{CCl}_4$	24	0
7	0.02	THF	24	0
8	0.02	<i>n</i> -Hexane	24	0
9	0.02	EtOAc	3	65
10	0.02	DMF	3	55
11	0.02	$\text{CH}_3\text{CN}$	8	93
12	0.02	EtOH	8	95
13	0.02	MeOH	8	95
14 <sup>c</sup>	0.02	$\text{H}_2\text{O}$	8	Trace
15 <sup>d</sup>	0.02	$\text{H}_2\text{O}$	8	65
16 <sup>e</sup>	0.02	$\text{H}_2\text{O}$	8	95

<sup>a</sup> All reactions were carried out with styrene episulfide (1 mmol), phenylacetylene (1 mmol) and sodium azide (1.2 mmol) at room temperature. <sup>b</sup> Isolated yields. <sup>c</sup> Catalysed by  $\text{NiFe}_2\text{O}_4$ . <sup>d</sup> Catalysed by  $\text{NiFe}_2\text{O}_4@\text{SiO}_2$ . <sup>e</sup> Catalysed by Cu nanoparticles.

O stretching vibrations also appears in this region, which probably overlaps with the absorption band at  $468\text{ cm}^{-1}$  and leads to an increase in its intensity.<sup>45</sup>

**3.1.3. X-ray diffraction (XRD).** The X-ray diffraction (XRD) patterns of  $\text{NiFe}_2\text{O}_4$ ,  $\text{NiFe}_2\text{O}_4@\text{SiO}_2$  and  $\text{NiFe}_2\text{O}_4@\text{SiO}_2\text{-Cu}$  nanoparticles are illustrated in Fig. 3. As shown, all the peaks of  $\text{NiFe}_2\text{O}_4$ ,  $\text{SiO}_2$  and Cu particles are detectable. The diffraction peaks at  $2\theta = 18.55^\circ$ ,  $30.42^\circ$ ,  $35.80^\circ$ ,  $37.46^\circ$ ,  $43.49^\circ$ ,  $53.92^\circ$ ,  $57.48^\circ$ ,  $63.11^\circ$  and  $74.13^\circ$  correspond to (111), (220), (311), (222), (400), (422), (511), (440) and (622) crystal planes of  $\text{NiFe}_2\text{O}_4$ , which confirm the synthesis of pure and crystalline  $\text{NiFe}_2\text{O}_4$  nanoparticles. These peaks are compatible with the standard data (JCPDS 01-074-2081).<sup>43</sup>

The same patterns of characteristic peaks can be seen for  $\text{NiFe}_2\text{O}_4@\text{SiO}_2$ , indicating that the embedded magnetite cores keep their crystalline phase after  $\text{SiO}_2$  covering. The diffraction peaks of Cu situated at  $2\theta = 43.7^\circ$ ,  $50.7^\circ$ , and  $74.3^\circ$  are related to the (111), (200), and (220) planes of the fcc structure, respectively and they are in agreement with copper standard (JCPDS 04-0836).<sup>44</sup> The average crystallite size of nanoparticles is calculated using the Scherrer's formula (36 nm).

**3.1.4. TEM and FESEM of  $\text{NiFe}_2\text{O}_4@\text{SiO}_2\text{-Cu}$ .** The morphology and size distribution of the as-prepared

nanocomposite were checked by TEM and FESEM methods. TEM images of  $\text{NiFe}_2\text{O}_4@\text{SiO}_2\text{-Cu}$  show the cores of nickel ferrite surrounded by the black silica layers. The copper nanoparticles are also visible as dark grains immobilized on silica layer (Fig. 4).

FESEM images of  $\text{NiFe}_2\text{O}_4$ ,  $\text{NiFe}_2\text{O}_4@\text{SiO}_2$  and  $\text{NiFe}_2\text{O}_4@\text{SiO}_2\text{-Cu}$  are shown in Fig. 5. These images provide more detailed information on the morphology of the synthesized magnetic nanocomposite. As can be seen, the surface of the ferrite is completely covered by  $\text{SiO}_2$ , and nickel ferrite particles are camouflaged under silica layers. In addition, the copper nanoparticles immobilized on the monodispersed  $\text{NiFe}_2\text{O}_4@\text{SiO}_2$  spheres are clearly visible in the images. The presence of nanoparticles with diameters ranging from 20 to 44 nm is confirmed through FESEM images. The obtained results are completely consistent with TEM and XRD data.

**3.1.5. EDS of  $\text{NiFe}_2\text{O}_4@\text{SiO}_2\text{-Cu}$ .** The chemical composition of  $\text{NiFe}_2\text{O}_4@\text{SiO}_2\text{-Cu}$  with weight and atomic percentage of the elements were detected using EDS technique and elemental mapping patterns. This analysis confirms the presence of Cu, Ni, Fe, Si and O elements in the structure of nanocomposite (Fig. 6). The higher peak intensity of Si element compared to Fe and Ni peaks indicates that  $\text{NiFe}_2\text{O}_4$  nanoparticles are trapped by  $\text{SiO}_2$  and confirms the synthesized core-shell structure of  $\text{NiFe}_2\text{O}_4@\text{SiO}_2$ . The exact concentration of Ni, Fe and Cu was determined by ICP-OES and the resulting amounts were 2.01, 3.38 and 2.35 wt% respectively, which are in high agreement with EDS data.

### 3.2. Synthesis of $\beta$ -thiol-1,2,3-triazoles catalyzed by $\text{NiFe}_2\text{O}_4@\text{SiO}_2\text{-Cu}$

The reaction conditions of the one-pot click synthesis of 2-phenyl-2-(4-phenyl-1*H*-1,2,3-triazol-1-yl)ethane-1-thiol from styrene episulfide, sodium azide and phenyl acetylene was optimized applying different conditions.

The various factors such as solvent, reaction time and quantity of catalyst and reactant were investigated. The results obtained are summarized in Table 1. The most satisfactory outcome was achieved using styrene episulfide (1 mmol), phenylacetylene (1 mmol), sodium azide (1.2 mmol) and  $\text{NiFe}_2\text{O}_4@\text{SiO}_2\text{-Cu}$  (0.02 g) as catalyst in water at room temperature (Table 1, entry 4).

It is important that in the absence of the catalyst, the reaction showed no improvement even after 20 h (entry 1). In order to optimize the catalyst quantity, the model reaction was tested utilizing different amounts of catalyst (0.01, 0.015, 0.02 and 0.03 g), and the desired result was obtained using 0.02 g. Increasing the catalyst quantity from 0.015 to 0.02 g not only decreased the reaction time but also increased the product yield (entries 2–4). Using more amounts of the catalyst did not affect the triazole yield (entry 5).

In order to study the effect of solvent, the model reaction was carried out in various solvents. The results revealed that the polar solvents were practical and useful whereas non-polar solvents were not appropriate to accomplish the reaction (entries 6–13).



**Table 2** Regioselective one-pot synthesis of  $\beta$ -thiol-1,2,3-triazoles from thiiranes catalysed by  $\text{NiFe}_2\text{O}_4/\text{SiO}_2\text{-Cu}^a$ 

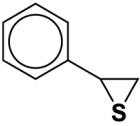
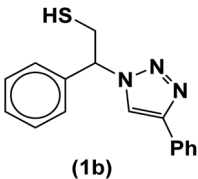
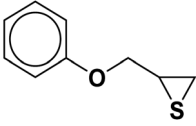
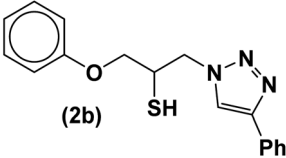
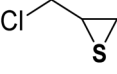
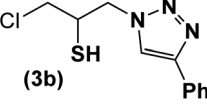
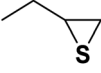
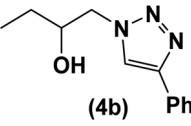
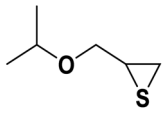
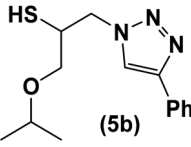
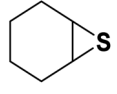
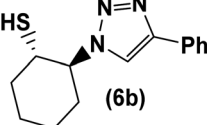
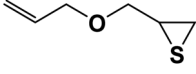
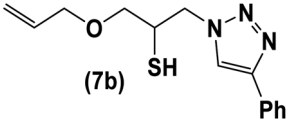
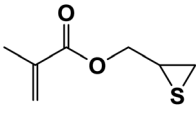
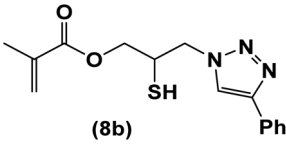
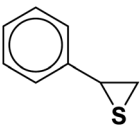
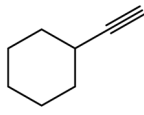
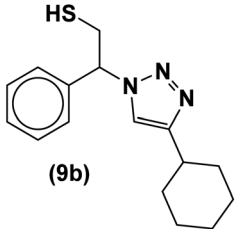
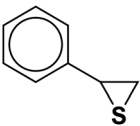
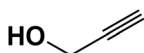
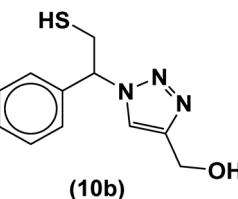
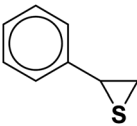
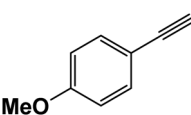
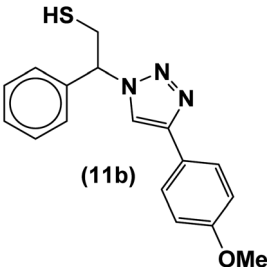
Entry	Thiirane (a)	Alkyne	Triazole (b)	Time (h)	Yield <sup>b</sup> (%)	m.p. <sup>45</sup> (°C)
1		$\text{Ph}-\text{C}\equiv\text{C}-\text{H}$	 (1b)	8	98	122–124
2		$\text{Ph}-\text{C}\equiv\text{C}-\text{H}$	 (2b)	9	90	113–114
3		$\text{Ph}-\text{C}\equiv\text{C}-\text{H}$	 (3b)	8.5	82	154–157
4		$\text{Ph}-\text{C}\equiv\text{C}-\text{H}$	 (4b)	10	94	104–106
5		$\text{Ph}-\text{C}\equiv\text{C}-\text{H}$	 (5b)	9	89	74–75
6		$\text{Ph}-\text{C}\equiv\text{C}-\text{H}$	 (6b)	8	93	156–159
7		$\text{Ph}-\text{C}\equiv\text{C}-\text{H}$	 (7b)	8.5	90	70
8		$\text{Ph}-\text{C}\equiv\text{C}-\text{H}$	 (8b)	8	81	86–92
9			 (9b)	10	90	125–128
10			 (10b)	9.5	92	101–105





Table 2 (Contd.)

Entry	Thiirane (a)	Alkyne	Triazole (b)	Time (h)	Yield <sup>b</sup> (%)	m.p. <sup>45</sup> (°C)
11				8.5	96	130–132

<sup>a</sup> All reactions were carried out with 1 mmol of thiirane in the presence of alkyne (1 mmol), sodium azide (1.2 mmol) and nano-NiFe<sub>2</sub>O<sub>4</sub>@SiO<sub>2</sub>-Cu (0.02 g) in water at room temperature. <sup>b</sup> Yields refer to isolated pure products.

Water as an abundant, green and eco-friendly solvent is superior to other solvents, and it was chosen as the favorable option (entry 4).

In order to evaluate the catalytic activity of the catalyst components, the model reaction was investigated separately using NiFe<sub>2</sub>O<sub>4</sub>, NiFe<sub>2</sub>O<sub>4</sub>@SiO<sub>2</sub> and Cu under the optimal conditions (entries 14–16). The results showed that although the presence of NiFe<sub>2</sub>O<sub>4</sub> and SiO<sub>2</sub> in the catalyst structure increased the efficiency of the catalyst, copper nanoparticles played the most significant role in this regard. The highest product yield can be achieved in the presence of NiFe<sub>2</sub>O<sub>4</sub>@SiO<sub>2</sub>-Cu because the synergistic effect between components greatly improves the catalytic activity and selectivity.

The usability and generality of this research were investigated by the reaction of structurally diverse thiiranes with either electron-donating or withdrawing substituents and cyclic thiiranes in the presence of phenylacetylene, sodium azide and NiFe<sub>2</sub>O<sub>4</sub>@SiO<sub>2</sub>-Cu nanocatalyst under the optimum conditions (Table 2, entries 1–8). The reaction of some other alkynes such as aliphatic terminal alkynes and 4-methoxyphenyl acetylene

with styrene episulfide was also examined under the optimized conditions (entries 9–11). The results show that all reactions were performed successfully within 8–10 h to give the corresponding 1,2,3-triazoles in 81–98% yields.

### 3.3. Recycling of NiFe<sub>2</sub>O<sub>4</sub>@SiO<sub>2</sub>-Cu catalyst

The other green aspect of this method was also investigated by the reusability of NiFe<sub>2</sub>O<sub>4</sub>@SiO<sub>2</sub>-Cu magnetic nanoparticles in one-pot synthesis of 2-phenyl-2-(4-phenyl-1*H*-1,2,3-triazol-1-yl)ethane-1-thiol from styrene episulfide, sodium azide and phenyl acetylene under the optimized reaction conditions (Table 2, entry 1). After completion of the reaction, the nanoparticles were easily separated and collected by an external magnet, washed with ethyl acetate and then dried to use in the next cycles. The catalyst can be reused several times without the considerable loss of catalytic activity (Fig. 7). Furthermore, to study the reusability and persistence of NiFe<sub>2</sub>O<sub>4</sub>@SiO<sub>2</sub>-Cu particles, VSM, FESEM, FT-IR and TEM of the recycled catalyst were studied. The results showed that the structure of nanocatalyst was almost stable even after four runs (Fig. 8).

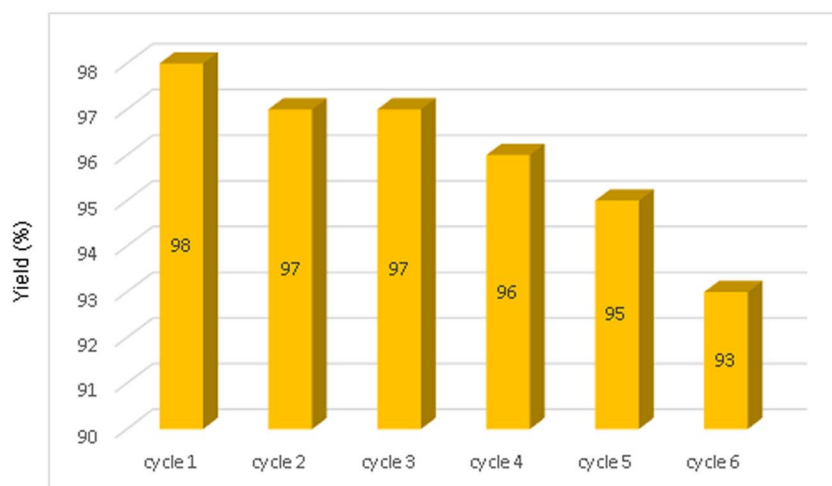


Fig. 7 Recycling of NiFe<sub>2</sub>O<sub>4</sub>@SiO<sub>2</sub>-Cu in the synthesis of 2-phenyl-2-(4-phenyl-1*H*-1,2,3-triazol-1-yl)ethane-1-thiol.



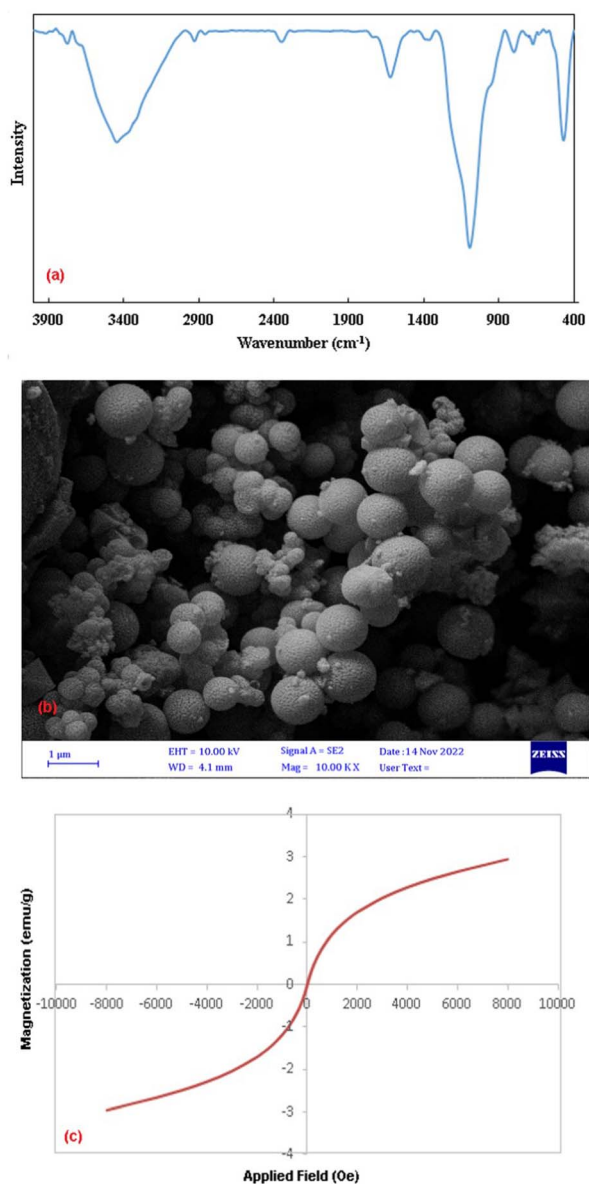


Fig. 8 (a) FT-IR, (b) FESEM and (c) VSM of  $\text{NiFe}_2\text{O}_4@\text{SiO}_2\text{-Cu}$  after four runs.

The extent of Ni, Fe and Cu leaching during catalytic reactions was investigated by ICPOES analysis of the supernatant liquid after removal of the catalyst. The results confirmed the absence of metals in the supernatant liquid.

### 3.4. Hot filtration test

The heterogeneity of the catalyst was confirmed through the hot filtration test. For this purpose, the catalyst was filtered after 2 hours in the model reaction at 100 °C, and the filtrate was allowed to react for additional 10 hours, but no progress of the reaction was seen in the absence of the catalyst, indicating no leakage of the catalyst into the reaction mixture. Therefore,  $\text{NiFe}_2\text{O}_4@\text{SiO}_2\text{-Cu}$  is heterogeneous and is essential to perform the cyclization reaction.

### 3.5. Comparison of $\text{NiFe}_2\text{O}_4@\text{SiO}_2\text{-Cu}$ catalytic activity with other catalysts

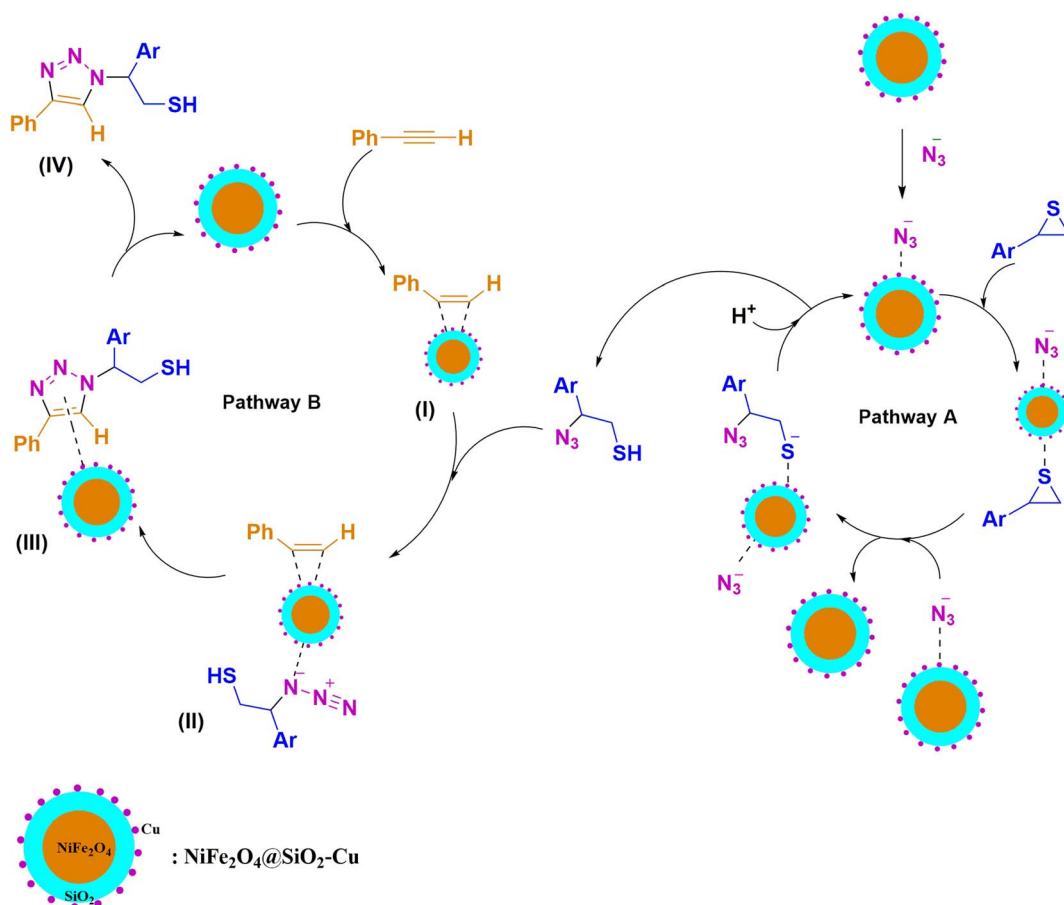
The click synthesis of 1,2,3-triazole from thiiranes is a new topic and has not been considered so far, except in two recent cases reported by the authors of this paper.<sup>44,45</sup> The privileges of the mentioned method were revealed by comparing the 1,3-dipolar reaction of styrene episulfide, phenyl acetylene and sodium azide in the presence of  $\text{NiFe}_2\text{O}_4@\text{SiO}_2\text{-Cu}$  with the other two previously reported catalysts. In terms of temperature, recyclability and product yield, the present procedure is more favorable. The reaction is carried out in the presence of  $\text{NiFe}_2\text{O}_4@\text{SiO}_2\text{-Cu}$  at room temperature and the product is obtained with higher yield. The most important advantage of this method is the completion of the reaction at low temperature under mild conditions, which indicates the higher efficiency of the newly synthesized nanocatalyst.

### 3.6. The proposed mechanism for regioselective synthesis of $\beta$ -thiol-1,2,3-triazoles catalyzed by $\text{NiFe}_2\text{O}_4@\text{SiO}_2\text{-Cu}$

The possible mechanism for the synthesis of  $\beta$ -thiol-1,2,3-triazole involves two pathways (A) and (B) (Scheme 3).  $\text{NiFe}_2\text{O}_4@\text{SiO}_2\text{-Cu}$  simultaneously catalyzes both cleavage of the thiirane ring and 1,3-dipolar cycloaddition to produce triazoles.<sup>39,45</sup> First, a non-covalent interaction is established between the azide and the metal of catalyst, and then the thiirane ring is activated by the catalyst through its Lewis acid property. Next, the azide is transferred from the catalyst and the ring opening of thiirane occurs to produce 2-azido-2-arylethanethiol (pathway A). In this pathway, the cleavage of thiirane rings is regioselective and thiiranes bearing aryl substituents due to the stability of benzyl carbocation prefer to be opened from the more hindered position *via*  $\text{S}_{\text{N}}1$  type of mechanism ( $\alpha$ -cleavage); while the thiiranes with alkyl and allyl groups are effectively opened from less hindered place *via*  $\text{S}_{\text{N}}2$  type of mechanism ( $\beta$ -cleavage). In this pathway, the catalytic effect of  $\text{NiFe}_2\text{O}_4@\text{SiO}_2\text{-Cu}$  was examined through the reaction between styrene episulfide and sodium azide in the absence of catalyst, and it was revealed that, only a very small amount of 2-azido-2-arylethanethiol had been produced. Consumption of reactants and also the production of 2-azido-2-phenylethanethiol intermediate were tracked by gas chromatography (GC) method and thin layer chromatography (TLC) runs of the reaction mixture, and it was found that 2-azido-2-arylethanethiol is rapidly formed, therefore, the 1,3-dipolar cycloaddition step is the rate-determining step (RDS).

In pathway B, initially, the terminal alkyne is activated through  $\pi$ -complexation with catalyst to give intermediate (I).<sup>67</sup> Then, the reaction of 2-azido-2-phenylethanethiol produced in pathway A with intermediate (I) leads to generate the intermediate (II), and 1,2,3-triazole (III) is subsequently created from the 1,3-dipolar cycloaddition between azide and intermediate (II). The consumption of the alkyne as well as the disappearing of the 2-azido-2-arylethanethiol intermediate, were monitored by the GC and TLC of the reaction mixture. Eventually, the





Scheme 3 The mechanism proposed for the regioselective synthesis of  $\beta$ -thiol-1,2,3-triazole catalyzed by  $\text{NiFe}_2\text{O}_4$ @ $\text{SiO}_2$ -Cu.

catalyst nanoparticles were separated from intermediate (III), and 1,2,3-triazole (IV) was obtained.

## 4. Conclusions

In conclusion, the  $\text{NiFe}_2\text{O}_4$ @ $\text{SiO}_2$ -Cu nanocomposite as a new magnetic nanocatalyst was successfully synthesized and characterized using various analytical techniques such as FT-IR, XRD, FESEM, EDS, ICP-OES, TEM, and VSM. Its unique efficacy in organic synthesis was investigated through a one-pot multi-component reaction for the synthesis of diverse  $\beta$ -thiol-1,4-disubstituted-1,2,3-triazoles, which hold chemical and potential biological significance, *via* a reaction involving sodium azide, terminal alkyne, and aliphatic/aromatic/cyclic thiiranes. The application of this nanocomposite in the aforementioned reaction resulted in the production of pure products with high yields, and acceptable reaction times. The current method proves highly suitable for obtaining a broad scope of 1,2,3-triazoles, which are considered valuable heterocyclic compounds in the pharmaceutical field. Furthermore, the as-prepared nanocatalyst demonstrated excellent recyclability, as it was easily recovered from the reaction mixture using an external magnet and reused for four consecutive runs. Overall, the notable characteristics of this approach encompass the utilization of the reusable catalytic system, one-pot procedure,

mild reaction conditions, perfect regioselectivity, green solvent, readily accessible starting reactants, and effortless product filtration, as well as high yields of the target products. These privileged characteristics make this new approach environmentally attractive and cost effective.

## Conflicts of interest

There are no conflicts to declare.

## Acknowledgements

The financial support of this work by the Research Council of Payame Noor University is gratefully acknowledged.

## References

- 1 S. Saranya, K. R. Rohit, S. Radhika and G. Anilkumar, *Org. Biomol. Chem.*, 2019, **17**, 8048.
- 2 L. M. Ramos, M. O. Rodrigues and B. A. D. Neto, *Org. Biomol. Chem.*, 2019, **17**, 7260.
- 3 K. K. Das, S. Manna and S. Panda, *Chem. Commun.*, 2021, **57**, 441.
- 4 L. Biesen and T. J. J. Müller, *Adv. Synth. Catal.*, 2021, **363**, 980.



- 5 D. Insuasty, J. Castillo, D. Becerra, H. Rojas and R. Abonia, *Molecules*, 2020, **25**, 505.
- 6 A. Ashraf, Z. Shafiq, K. Mahmood, M. Yaqub and W. Rauf, *RSC Adv.*, 2020, **10**, 5938.
- 7 A. Singh, N. A. Mir, S. Choudhary, D. Singh, P. Sharma, R. Kantc and I. Kumar, *RSC Adv.*, 2018, **8**, 15448.
- 8 S. A. R. Mulla, M. Y. Pathan, S. S. Chavan, S. P. Gamble and D. Sarkar, *RSC Adv.*, 2014, **4**, 7666.
- 9 J. C. Flores-Reyes, V. C. Cotlame-Salinas, I. A. Ibarra, E. González-Zamora and A. Islas-Jácome, *RSC Adv.*, 2023, **13**, 16091.
- 10 R. Javahershenas and S. Nikzat, *RSC Adv.*, 2023, **13**, 16619.
- 11 M. Rimaz, B. Khalili, G. Khatyal, H. Mousavi and F. Aali, *Aust. J. Chem.*, 2017, **70**, 1274.
- 12 C. Wang, Q. Li, S. Wang, G. Zhu, A. Zhu and L. Li, *RSC Adv.*, 2021, **11**, 38108.
- 13 S. Mukherjee, J. W. Yang, S. Hoffmann and B. List, *Chem. Rev.*, 2007, **107**, 547.
- 14 D.-H. Jhuo, B.-C. Hong, C.-W. Chang and G.-H. Lee, *Org. Lett.*, 2014, **16**, 2724.
- 15 Y. Hayashi, H. Gotoh, T. Hayashi and M. Shoji, *Angew. Chem.*, 2005, **117**, 4284.
- 16 M. Marigo, T. C. Wabnitz, D. Fielenbach and K. A. Jørgensen, *Angew. Chem.*, 2005, **117**, 804.
- 17 D. Enders, M. R. M. Huttl, C. Grondal and G. Raabe, *Nature*, 2006, **441**, 861.
- 18 M. F. Mady, G. E. A. Awad and K. B. Jørgensen, *Eur. J. Med. Chem.*, 2014, **84**, 433.
- 19 H. N. Hafez, H. A. Abbas and A. R. El-Gazzar, *Acta Pharm.*, 2008, **58**, 359.
- 20 M. D. Chen, S. J. Lu, G. P. Yuag, S. Y. Yang and X. L. Du, *Heterocycl. Commun.*, 2000, **6**, 421.
- 21 F. C. Silva, M. C. B. V. de Souza, I. I. P. Frugulhetti, H. C. Castro, S. L. d. O. Souza, T. M. L. de Souza, D. Q. Rodrigues, A. M. T. Souza, P. A. Abreu, F. Passamani, C. R. Rodrigues and V. F. Ferreira, *Eur. J. Med. Chem.*, 2009, **44**, 373.
- 22 A. Kamal, S. Prabhakar, M. J. Ramaiah, P. V. Reddy, C. R. Reddy, A. Mallareddy, N. Shankaraiah, T. L. N. Reddy, S. N. C. V. L. Pushpavalli and M. Pal-Bhadra, *Eur. J. Med. Chem.*, 2011, **46**, 3820.
- 23 K. M. Banu, A. Dinaker and C. Ananthnarayan, *Indian J. Pharm. Sci.*, 1999, **61**, 202.
- 24 G. Ravi, A. R. Nath, A. Nagaraj, S. Damodhar and G. N. Rao, *Der Pharma Chemica*, 2014, **6**, 223.
- 25 T. W. Kim, Y. Yong, S. Y. Shin, H. Jung, K. H. Park, Y. H. Lee, Y. Lim and K. Y. Jung, *Bioorg. Chem.*, 2015, **59**, 1.
- 26 R. Raj, P. Singh, P. Singh, J. Gut, P. J. Rosenthal and V. Kumar, *Eur. J. Med. Chem.*, 2013, **62**, 590.
- 27 R. Eisavi and A. Karimi, *RSC Adv.*, 2019, **9**, 29873.
- 28 F. Alonso, Y. Moglie, G. Radivoy and M. Yus, *J. Org. Chem.*, 2011, **76**, 8394.
- 29 F. Alonso, Y. Moglie, G. Radivoy and M. Yus, *Adv. Synth. Catal.*, 2010, **352**, 3208.
- 30 H. Sharghi, M. H. Beyzavi, A. Safavi, M. M. Doroodmand and R. Khalifeh, *Adv. Synth. Catal.*, 2009, **351**, 2391.
- 31 J. S. Yadav, B. V. S. Reddy, G. M. Reddy and D. N. Chary, *Tetrahedron Lett.*, 2007, **48**, 8773.
- 32 T. Boningari, A. Olmos, B. M. Reddy, J. Sommer and P. Pale, *Eur. J. Org. Chem.*, 2010, **2010**, 6338.
- 33 H. Sharghi, M. Hosseini-Sarvari, F. Moeini, R. Khalifeh and A. S. Beni, *Helv. Chim. Acta*, 2010, **93**, 435.
- 34 B. S. P. Anil Kumar, K. Harsha Vardhan Reddy, G. Satish, R. Uday Kumar and Y. V. D. Nageswar, *RSC Adv.*, 2014, **4**, 60652.
- 35 H. Naeimi and V. Nejadshafiee, *New J. Chem.*, 2014, **38**, 5429.
- 36 K. Rajender Reddy, C. Uma Maheswari, K. Rajgopal and M. Lakshmi Kantam, *Synth. Commun.*, 2008, **38**, 2158.
- 37 H. Esmacili-Shahri, H. Eshghi, J. Lari and S. A. Rounaghi, *Appl. Organomet. Chem.*, 2018, **32**, e3947.
- 38 N. Noshiranzadeh, M. Emami, R. Bikas and A. Kozakiewicz, *New J. Chem.*, 2017, **41**, 2658.
- 39 H. Sharghi and I. Ghaderi, *Org. Chem. Res.*, 2017, **3**, 162.
- 40 H. Sharghi, A. Khoshnood, M. M. Doroodmand and R. Khalifeh, *J. Iran. Chem. Soc.*, 2012, **9**, 231.
- 41 H. Sharghi, S. Ebrahimpourmoghaddam, M. M. Doroodmand and A. Purkhosrow, *Asian J. Org. Chem.*, 2012, **1**, 377.
- 42 G. Kumaraswamy, K. Ankamma and A. Pitchaiah, *J. Org. Chem.*, 2007, **72**, 9822.
- 43 J. Lu, E. Q. Ma, Y. H. Liu, Y. M. Li, L. P. Mo and Z. H. Zhang, *RSC Adv.*, 2015, **5**, 59167.
- 44 R. Eisavi and K. Naseri, *RSC Adv.*, 2021, **11**, 13061.
- 45 R. Eisavi and F. Ahmadi, *Sci. Rep.*, 2022, **12**, 11939.
- 46 M. Boudart, *Chem. Rev.*, 1995, **95**, 661.
- 47 H. Hattori, *Chem. Rev.*, 1995, **95**, 537.
- 48 M. R. Othman, Z. Helwani, Martunus and W. J. N. Fernando, *Appl. Organomet. Chem.*, 2009, **23**, 335.
- 49 E. J. Ras and G. Rothenberg, *RSC Adv.*, 2014, **4**, 5963.
- 50 M. Gilanizadeh and B. Zeynizadeh, *Res. Chem. Intermed.*, 2020, **46**, 2962.
- 51 V. Polshettiwar, R. Luque, A. Fihri, H. Zhu, M. Bouhrara and J. M. Basset, *Chem. Rev.*, 2011, **111**, 3036.
- 52 T. Wang, L. Zhang, H. Wang, W. Yang, Y. Fu, W. Zhou, W. Yu, K. Xiang, Z. Su, S. Dai and L. Chai, *ACS Appl. Mater. Interfaces*, 2013, **5**, 12449.
- 53 M. Kumar, H. S. Dosanjh, Sonika, J. Singh, K. Monira and H. Singh, *Environ. Sci.: Water Res. Technol.*, 2020, **6**, 491.
- 54 R. Verma, K. R. B. Singh, R. Verma and J. Singh, *Luminescence*, 2023, **38**, 1393.
- 55 J. Singh, K. R. B. Singh, M. Kumar, R. Verma, R. Verma, P. Malik, S. Srivastava, R. P. Singh and D. Kumar, *Mater. Adv.*, 2021, **2**, 6665.
- 56 K. R. B. Singh, V. Nayak, J. Singh, A. K. Singh and R. P. Singh, *RSC Adv.*, 2021, **11**, 24722.
- 57 R. G. Kerry, K. R. B. Singh, S. Mahari, A. Bihari Jena, B. Panigrahi, K. C. Pradhan, S. Pal, B. Kisan, J. Dandapat, J. Singh, S. S. Pandey, R. P. Singh and S. Majhi, *OpenNano*, 2023, **10**, 100126.
- 58 J. Patel, K. R. B. Singh, A. K. Singh, J. Singh and A. K. Singh, *Environ. Res.*, 2023, **235**, 116674.
- 59 S. Hassanzadeh, R. Eisavi and M. Abbasian, *Appl. Organomet. Chem.*, 2018, **32**, e4520.





- 60 R. Eisavi and S. Alifam, *Phosphorus, Sulfur Silicon Relat. Elem.*, 2017, **193**, 211.
- 61 R. Eisavi, S. Ghadernejad, B. Zeynizadeh and F. M. Aminzadeh, *J. Sulfur Chem.*, 2016, **37**, 537.
- 62 R. Eisavi, F. Ahmadi, B. Ebadzade and S. Ghadernejad, *J. Sulfur Chem.*, 2017, **38**, 614.
- 63 S. Hassanzadeh, R. Eisavi and M. Abbasian, *J. Sulfur Chem.*, 2019, **40**, 240.
- 64 M. Mahmoudzadeh, E. Mehdipour and R. Eisavi, *J. Coord. Chem.*, 2019, **72**, 841.
- 65 R. Eisavi and B. Zeynizadeh, *Phosphorus, Sulfur Silicon Relat. Elem.*, 2016, **191**, 65.
- 66 F. Rubio, J. Rubio and J. L. Oteo, *Spectrosc. Lett.*, 1998, **31**, 199.
- 67 Y. Fang, K. Bao, P. Zhang, H. Sheng, Y. Yun, S. X. Hu, D. Astruc and M. Zhu, *J. Am. Chem. Soc.*, 2021, **143**, 1768.

